Ordering Transitions of Liquid Crystals Triggered by Metal Oxide-Catalyzed Reactions of Sulfur Oxide Species

Nanqi Bao,^{+,‡} Jake I. Gold,^{#,‡} Jonathan K. Sheavly,[#] James J. Schauer,^{†,#} Victor M. Zavala,[#] Reid C. Van Lehn,[#] Manos Mavrikakis*,[#] and Nicholas L. Abbott*,⁺

*Smith School of Chemical and Biomolecular Engineering, Cornell University, Ithaca, NY 14853, USA

ABSTRACT: Liquid crystals (LCs), when supported on reactive surfaces, undergo changes in ordering that can propagate over distances of micrometers, thus providing a general and facile mechanism to amplify atomic-scale transformations on surfaces into the optical scale. While reactions on organic and metal substrates have been coupled to LC ordering transitions, metal oxide substrates, which offer unique catalytic activities for reactions involving atmospherically important chemical species such as oxidized sulfur species, have not been explored. Here we investigate this opportunity by designing LCs that contain 4'-cyanobiphenyl-4-carboxylic acid (CBCA) and respond to surface reactions triggered by parts-per-billion concentrations of SO₂ gas on anatase (101) substrates. We used electronic structure calculations to predict that the carboxylic acid group of CBCA binds strongly to anatase (101) in a perpendicular orientation, a prediction that we validated in experiments in which CBCA (0.005 mol%) was doped into a LC (4'-n-pentyl-4-biphenylcarbonitrile). Both experiment and computational modeling further demonstrated that SO₃-like species, produced by a surface-catalyzed reaction of SO₂ with H₂O on anatase (101), displace CBCA from the anatase surface, resulting in an orientational transition of the LC. Experiments also reveal the LC response to be highly selective to SO₂ over other atmospheric chemical species (including H₂O, NH₃, H₂S, and NO₂), in agreement with our computational predictions for anatase (101) surfaces. Overall, we establish that the catalytic activities of metal oxide surfaces offer the basis of a new class of substrates that trigger LCs to undergo ordering transitions in response to chemical species of relevance to atmospheric chemistry.

INTRODUCTION

Materials that can be programmed to respond to targeted chemical species1 have broad potential utility, including for energy transduction,^{2,3} amplification of chemical information⁴ and design of autonomous and adaptive chemical systems.^{5,6} A key challenge underlying the encoding of chemical responsiveness in organic materials (e.g., polymer thin films, hydrogels, liquid crystals) is understanding how changes in composition and atomic-scale structure of interfaces impact functional properties.⁷⁻¹² Liquid crystals (LCs),¹³ for example, can be oriented by short-range (chemically specific) and longrange (e.g., electrical double layer) interactions between the molecules forming the LC (or molecular dopants in the LCs) and chemical functional groups presented at confining surfaces. 14-21 The orientation-dependence of these interactions is weak (typically 10⁻³-10⁻² mJ/m²) and, therefore, LC ordering is readily perturbed by changes in the structure of surfaces that accompany reactions. 16,22 In this paper, we focus on ordering transitions in LC materials triggered by catalytic reactions occurring on metal oxide surfaces that involve sulfur oxide species of relevance to atmospheric chemistry.²³

Sulfur dioxide (SO₂) is a widely used industrial chemical²⁴ and is a major component of the atmospheric sulfur cycle, contributing to acid deposition and sulfate aerosol that affect both climate and human health.^{25,26} Nearly one-half of global

SO₂ emissions are converted to particulate sulfate by ozone, hydrogen peroxide, and OH radicals.^{27,28} The transformation of SO₂ can occur in the gas phase, in water droplets,^{28,29} or via heterogenous processes on mineral aerosol surfaces (e.g., TiO₂, Fe₂O₃ and Al₂O₃).^{30,31} TiO₂, in particular, is present in airborne particulate matter.³² The catalytic transformation of SO₂ on TiO₂ surfaces to other sulfur species (e.g., sulfite or sulfate) is impacted by various environmental conditions, including relative humidity, UV irradiation and molecular oxygen.³² Here, we explore how atomic-scale transformations of SO₂ on metal oxide surfaces can be coupled to LC ordering transitions, thus providing new knowledge for how surface-catalyzed reactions of relevance to atmospheric chemistry can be targeted to generate macroscopic changes in material properties.

The work reported in this paper advances the design of chemically-responsive LCs. A number of approaches to the design of chemically responsive LCs have been reported. 33-49 One strategy leverages changes in the organization of LCs upon exposure to targeted chemical species. For example, chiral molecules that change their helical twisting power upon interaction with targeted chemical species have been doped into cholesteric LCs. 33,34,42-49 Our work contributes to a second strategy that is based on surface-induced changes in LC ordering. For example, past studies have shown that ligand exchange reactions (e.g., nitrile or pyrimidine) at metal cation-

^{*}Department of Chemical and Biological Engineering, University of Wisconsin-Madison, Madison, WI 53706, USA

[†]Department of Civil and Environmental Engineering, University of Wisconsin-Madison, Madison, WI 53706, USA

decorated surfaces can be coupled to ordering transitions in LCs. ^{35–39} More recently, instead of using amorphous metal salt surfaces as substrates, LC systems have been designed to report atomic-scale processes such as dissociative adsorption of Cl₂ on the surfaces of crystalline metallic films (e.g., Pd on Au). ^{40,41} The catalytic activities of metal oxide surfaces, however, have not previously been explored for the design of chemically responsive LCs.

The chemical reactivities of metal oxide surfaces have been widely studied in surface science and catalysis and employed industrially (e.g., TiO₂, Al₂O₃, ZnO, and SnO₂⁵⁰⁻⁵⁴), and we set out to translate this understanding to the design of LCs that report in situ targeted atomic-scale surface processes. In particular, as mentioned above, TiO2 is studied as a photocatalyst in the context of atmospheric chemistry due to its high reactivity and abundance. 32,55 In addition to photochemical reactions, reactions involving H2O, sulfur-containing or nitrogen-containing molecules, and carboxylic acids⁵⁶ on TiO₂ have been extensively studied in the context of sensing,⁵⁷ energy storage, and conversion.⁵⁸ In this paper, we build from these prior studies to design LCs supported on TiO2 that respond to SO₂ and its reaction with H₂O. We comment that the anchoring of LCs on oxide surfaces has been reported (e.g., silica^{59,60} or indium tin oxide⁶¹), but chemically responsive LCs based on the catalytic activity of metal oxide surfaces have not been described.

To summarize, the work reported on this paper is conceptually important for two reasons. First, the paper is the first to report the design of a chemically responsive LC based on the catalytic reactivity of a metal oxide surface. We illustrate the approach using TiO₂ surfaces but emphasize that the approach is generalizable to a broad range of metal oxides with reactivities that are well-known from prior surface science, heterogeneous catalysis and atmospheric chemistry studies. 32,50-52 Second, this paper provides an approach that amplifies atomic-scale transformations involving SO₂ via LC ordering transitions, a chemical species that has not previously been shown to trigger ordering transitions in LCs. The optical response of the LC is sensitive to parts-per-billion (ppb) concentrations of SO₂, and highly selective to SO₂ over a range of other potentially interfering atmospheric compounds (e.g., H₂O vapor, NH₃, H₂S, and NO2). The LC ordering transitions triggered by SO2 on TiO₂ surfaces thus appears potentially promising as the basis of light-weight and energy efficient devices for atmospheric monitoring (using aerial drones or balloons⁶²) and for wearable sensors for monitoring of personal exposure to SO₂.48

METHODS

Experimental

Materials. Fischer's Finest glass slides, and solutions of sulfurous acid and sulfuric acid were purchased from Fischer Scientific (Pittsburgh, PA). Absolute ethanol (anhydrous, 200 proof) was purchased from Pharmco-AAPER (Brookfield, CT). All chemicals and solvents were of analytical reagent grade awere used as received. Deionized water possessed a resistivity of at least 18.2 M Ω cm or greater. Sulfuric acid (95-97%) and Nochromix cleaning agent were purchased from Sigma-Aldrich (Milwaukee, WI). The liquid crystals, 4'-n-pentyl-4-biphenylcarbonitrile (5CB) and 4-(trans-4'-pentylcyclohexyl)benzonitrile (PCH5) were purchased from Jiangsu Hecheng Advanced Materials Co., Ltd (Jiangsu, China). 4-(trans-4'-

propylcyclohexyl)-benzonitrile (PCH3) was synthesized using an approach reported previously. 63 4'-cyanobiphenyl-4-carboxylic acid (CBCA) was purchased from Matrix Scientific (Columbia, SC). 10 ± 0.5 ppm SO₂, 10 ± 0.7 ppm NO₂, 10 ± 1 ppm H₂S, 2% H₂ and 10 ± 0.6 ppm Cl₂ (balanced in nitrogen gas), and pure nitrogen gas (99.998% purity) were obtained from Airgas (Elmira, NY) and used as received.

Fabrication of TiO₂ thin films. We prepared TiO₂ thin films on three types of substrates. First, we used glass in experiments that required optically transparent substrates for polarized light microscopy of LCs. Second, we used silicon wafers in experiments that involved X-ray photoelectron spectroscopy (XPS) to minimize surface charging that can shift or broaden spectra.⁶⁴ Third, we used Pt-coated silicon substrates to enable infrared measurements using Fourier transformed polarizationmodulation infrared reflectance absorbance spectroscopy (PM-IRRAS) because the metal coating is reflective and provides surface selection rules that facilitate the interpretation of the IR spectra.65 For deposition of TiO2 films on glass, glass slides were cleaned using Nochromix cleaning solution (7g/100 mL Nochromix in deionized water and 100 mL sulfuric acid 97%) for 1 hour. Then, the slides were rinsed sequentially in deionized water and ethanol, and dried under a stream of nitrogen. For deposition of TiO₂ films on silicon wafers, wafers were rinsed in ethanol and dried under a stream of nitrogen. For deposition of TiO2 films on Pt-coated silicon substrates, thin films of Pt were fabricated by sequential deposition of 20 Å of Ti and 200 Å of Pt onto Si wafers using an electron beam evaporator. TiO₂ thin films were deposited on these three types of substrates using atomic layer deposition (ALD, Arradiance Gemstar-6) from tetrakis-dimethyl-amido titanium (TDMAT) and H₂O precursors at 225°C. The thickness of the TiO₂ film fabricated using 60 ALD cycles was measured to be 3.27±0.03 nm by ellipsometry (Woollam spectroscopic ellipsometer). TiO₂ thin films were then annealed at 500°C for 15 hours in dry air to obtain the anatase (101) phase (see SI for experimental

X-ray photoelectron spectroscopy (XPS). $\rm TiO_2$ anatase films formed on Si wafers (prepared as described above) were analyzed using a Scienta Omicron ESCA-2SR with operating pressure ~1x10-9 Torr. Monochromatic Al K α X-rays (1486.6 eV) were used, and photoelectrons were collected from a 5 mm diameter analysis area. Photoelectrons were collected at a 0° emission angle with a source to analyzer angle of 54.7°. A pass energy of 200 eV was used for wide/survey scans, and 50 eV was used for high-resolution scans. All XPS results were analyzed by CasaXPS software.

Fourier transformed polarization-modulation infrared reflectance absorbance spectroscopy (PM-IRRAS). IR spectra of CBCA films deposited onto anatase-coated Pt surfaces (prepared as described above) were obtained using a Nicolet Magna-IR 860 FT-IR spectrometer with a photoelastic modulator (PEM-90, Hinds Instruments, Hillsboro, OR), synchronous sampling demodulator (SSD-100, GWC Technologies, Madison, WI), and a liquid N₂-cooled mercury cadmium telluride (MCT) detector. All spectra (4000-700 cm⁻¹) were recorded at an incident angle of 83° with the modulation centered at either 2200 or 1600 cm⁻¹. For each sample, 500 scans were taken at a resolution of 4 cm⁻¹. Data were collected as differential reflectance vs. wavenumber. All IR results presented were analyzed by OMNIC software.

Formation of thin films of LC supported on anatase TiO₂. An 18 μ m-thick copper TEM grid (Electron Microscopy Sciences, Hatfield, PA) was placed on the anatase surface. The TEM grid had an overall diameter of 3 mm and was composed of square pores with lateral dimensions of 285 μ m. The grids were filled with 0.1 μ L LC using a microcapillary. The excess LC was removed from the grids by wicking the LC into an empty capillary tube.

Characterization of orientations of LCs in optical cells during gas exposure. LC samples hosted within TEM grids supported on anatase surfaces (fabricated on glass, see details above) were exposed to a stream of nitrogen containing SO2 within a flow cell that was constructed to direct the gaseous flow across the LC samples while permitting observation using a polarized-light microscope (CH40, Olympus, Melville, NY). A detailed description of the flow cell can be found in a prior publication.66 White light illumination was used in the microscopic observations. The stream of gas containing SO₂ was obtained from a certified cylinder (see Materials) containing 10 ppm SO₂ in nitrogen and diluted with N₂ to the desired concentrations (5 \pm 0.3, 2 \pm 0.1, 1 \pm 0.06, 0.5 \pm 0.03, 0.2 ± 0.01 , and 0.075 ± 0.005 ppm). The stream of gas containing NH₃, NO₂, H₂S or Cl₂ was obtained from a certified cylinder (see Materials) and diluted with N₂ to 5 ppm. The relative humidity of the N₂ was controlled using a dew point generator (LI-610, LI-COR Biosciences). The flow rate of each gas stream was controlled using a rotameter (Aalborg Instruments and Control, Orangeburg, NY). The total flow rate was maintained at 1000 mL/min at atmospheric pressure.

Theoretical

Density functional theory. Density functional theory (DFT) calculations were performed for bulk, surface, and cluster structures as implemented in Vienna Ab Initio Simulation Package (VASP code). 67,68 Projected augmented wave potentials were used to describe the electron-ion interactions.^{69,70} The exchange-correlation functional was described by the generalized gradient approximation (GGA-PBE).⁷¹ All calculations employed Grimme's D3 empirical dispersion correction scheme with zero damping.⁷² Spin polarization calculations were used for calculations that involved O2. The electron wave function was expanded using plane waves with an energy cutoff of 400 eV. The Brillouin zone (BZ) was sampled with Γ-centered Monkhorst-Pack kpoint mesh⁷³ with a k-point density greater than 11x11.4 kpoints per 1/Å. For example, on (2x3) surface unit cell of anatase (101) with dimensions of 11.0 Å x 7.6 Å, we used a kpoint mesh of 1 x 1 per unit cell. Gaussian smearing of 0.1 eV was used in all calculations. Structures were relaxed until the Hellmann-Feynman forces acting on each atom were less than 0.02 eV Å⁻¹. Dipole corrections were applied in the direction normal to the surface.74

The surface models of anatase TiO_2 were constructed from the most stable (101) facet that was confirmed in experiments (see Supporting Information (SI) for experimental evidence). Each TiO_2 slab contained four TiO_2 layers with the bottom two TiO_2 layers fixed to the bulk lattice constant of TiO_2 . The relaxed slab has a total thickness of 12.9 Å, defined as the difference in the atomic centers of the furthest atoms projected along the surface normal axis. The calculated lattice constants of anatase (a = 3.80 Å, b = 9.56 Å) are in good agreement with experimental values (a = 3.78 Å, b = 9.51 Å). A vacuum layer of at least 10 Å was

used as the separation between images of each slab. We used three types of unit cells, either (2x2), (2x3), or (2x4). Binding energy (BE) is calculated by: $BE = E_{anatase+ads} - E_{ads,g} - E_{anatase}$, where $E_{anatase+ads}$ is the total energy of the anatase (101) slab, including the adsorbate, $E_{ads,g}$ is the total energy of the adsorbate in the gas phase, $E_{anatase}$ is the total energy of the pristine anatase (101) slab with no adsorbate on it. By this definition, more negative values of BE correspond to stronger binding species. Reaction energies are calculated accordingly. Vibrational frequencies were calculated using the harmonic approximation. The mass-weighted Hessian was built up via numerical differentiation of the energy using a second-order finite difference approach 67,68 with a step size of 0.008 Å.

Molecular dynamics. Classical molecular dynamics (MD) simulations were performed to verify the homeotropic orientation of 5CB in the bulk induced by the CBCA anchored on anatase (101). 5CB was modeled using an all-atom model that was previously parameterized using DFT calculations and shown to reproduce the room temperature P_2 order parameter, density, and diffusivity.⁷⁶ CBCA was modeled following the same parameterization strategy used for 5CB by using the Generalized Amber Force Field⁷⁷ to model Lennard-Jones interactions and assigning atomistic partial charges using a gridbased electrostatic potential fitting method (see details in SI). TiO₂ surfaces were modeled using parameters obtained from prior ab initio simulations of TiO₂-water interfaces.⁷⁸ To model the molecules in the LC near an anatase (101) surface, CBCA molecules were bound to the surface by applying a position restraint and angle restraint, with parameters for the latter determined by fitting DFT-calculated binding energies as a function of angle to a harmonic potential. CBCA structures calculated from DFT relaxed to a tilt angle of 66° for the C-C bond that connects the phenyl ring and the carboxylic acid group of the CBCA molecule relative to the surface (see Figure 1 and Figure S5 for more details), which we define as being perpendicular in this work. Further details on the fitting procedure and the spring constants can be found in SI. Unbiased simulations were performed for a system consisting of 2000 5CB mesogens and 80 CBCA molecules bound to a 1.6 nm thick layer of anatase TiO2. The system was equilibrated utilizing a simulated annealing procedure before a 30 ns simulation was performed at 27°C and used to produce data. Additional details are included in SI. All MD simulations were performed using GROMACS 2016.⁷⁹

RESULTS AND DISCUSSION

Ordering of LC on Anatase (101)

We fabricated TiO₂ thin films with thicknesses of 3.27 ± 0.03 nm on glass substrates by ALD and then annealed the films at 500° C for 15 hours to obtain the anatase (101) phase, ⁸⁰ a result that was confirmed using X-ray diffraction (Figure S1a). We confirmed that the ALD films were continuous and smooth (root mean square roughness of 0.21 nm over an area of 2 μ m × 2 μ m from atomic force microscopy measurements (Figure S2)). The anatase (101) thin films used in this study did not contain detectable surface hydroxyl groups when characterized by PM-IRRAS (see details in Figure S1).

Previous studies have shown that SO₂ adsorbs strongly to TiO₂, as compared to other oxides, including Al₂O₃ or SiO₂, ⁸¹ and that its adsorption is influenced by H₂O. ^{82,83} Guided by these studies, we sought to use DFT to determine possible designs of

responsive LCs for SO₂ based on TiO₂ anatase (101) surfaces. We first evaluated the interactions of LCs, or potential dopants in LCs, with anatase (101), to predict the likely initial orientations of LCs on TiO₂ surfaces. Subsequently, we selected LCs and dopants with interactions that we predicted would be disrupted by reactions involving SO₂ that trigger an orientational transition of the LC on the TiO₂ surface.

We first evaluated the binding energy (BE) of 4'-n-pentyl-4biphenylcarbonitrile (5CB), a room temperature nematic LC, with TiO₂ surfaces by performing calculations with benzonitrile (PhCN, a surrogate molecule for 5CB, Figure 1 and Figure 2a). We calculated a BE of -0.74 eV between the nitrile group of PhCN and the undercoordinated Ti five-fold site (Ti^{5f}) on the anatase (101) surface when binding occurred in a perpendicular orientation (Figure 1 and Table 1). We also calculated the BE of H₂O to the Ti^{5f} site on anatase (101) to be 0.22 eV stronger than PhCN (BE = -0.96 eV, Table 1). This result suggests that under ambient conditions (20-60% relative humidity (RH)), 5CB on the TiO₂ anatase surface will be displaced by water and likely adopt a planar (parallel) orientation. To evaluate these predicted LC anchoring behaviors in experiments, we deposited an 18 µm-thick film of nematic 5CB onto the surface of an anatase film prepared as described above. Figure 2c shows that the 5CB exhibited a bright optical appearance in the ambient environment (40±10% RH), indicating a parallel or tilted orientation of 5CB on the surface (Figure 2e). This result is consistent with the computational predictions of preferential binding of H₂O over PhCN on anatase (101). We quantified the tilt angle of the LC from the surface normal by measuring the optical retardance of a film of 5CB between two anatase surfaces (see SI for additional details). The tilt angle was determined to be 85±7°. To confirm that the planar orientation of 5CB on anatase (101) is induced by the displacement of the LC by adsorbed H₂O (from ambient environment), we exposed a film of 5CB supported on the anatase surface to dry N₂. We observed 5CB to exhibit a dark optical appearance after 1 hourexposure to dry N₂ (Figure S7a), consistent with a sufficiently strong BE of PhCN (-0.76 eV) to induce homeotropic anchoring of the LC on the clean anatase surface. These results demonstrate that water controls the orientation of 5CB supported on anatase (101), leading us to search for a molecule with functional groups that would bind to TiO₂ more strongly than H₂O for the design of water-tolerant LCs under ambient humidity.

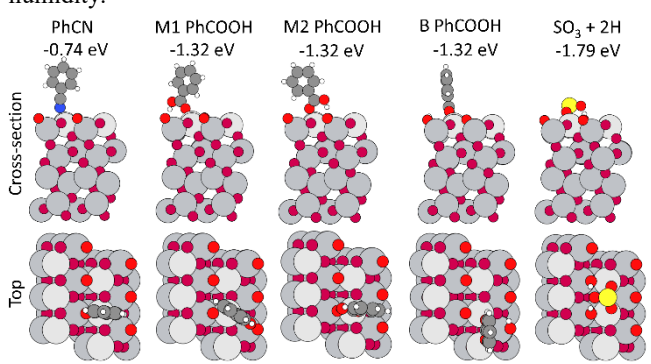


Figure 1. Top and cross-section view of the calculated minimum energy structure for PhCN, PhCOOH in a monodentate 1 (M1), monodentate 2 (M2), or bidentate (B) structure, and SO₃ + 2H* on (2x3) unit cell of anatase (101). Energies relative to the gas phase of clean anatase (101) and PhCN, PhCOOH, or SO₂+H₂O are shown below the structure name. Light gray is surface titanium,

light red is surface oxygen, white is hydrogen, blue is nitrogen, and yellow is sulfur. Subsurface atoms are colored with darker shades: dark gray is subsurface titanium, and dark red is subsurface oxygen.

Past studies have shown that carboxylic acid-containing molecules bind strongly to TiO2 surfaces, including anatase (101).84-88 Although there remains some debate over the structure of the bound carboxylic acids, it is generally believed that binding is monodentate, with the proton shuttling between carboxylate species and the bridge oxygen (Obr) on the anatase (101) surface. 84-88 Guided by this prior work, we explored the behavior of a carboxylic acid-containing molecule, 4'-cyano-4biphenylcarbolxylic acid (CBCA) on anatase (101). For calculations, we used PhCOOH as a surrogate molecule for CBCA (Figure 2b), and evaluated the BE of PhCOOH to anatase (101) in a perpendicular alignment using two monodentate structures (M1 and M2 in Figure 1) where O of COOH is bound to one Ti^{5f} site, and H of COOH is hydrogen bound to either the far O^{br} (M1) or the near O^{br} (M2). We also evaluated the bidentate structure (B in Figure 1) where the PhCOOH dissociates and binds to two Ti^{5f} sites through its O atoms, and the proton binds to a nearby Obr site, similar to the reported structure of PhCOOH on rutile.89 Interestingly, we found that the calculated BEs are similar for all three structures (BE = -1.32 eV in Figure 1). Because prior experimental studies suggest that carboxylic acid-containing species bind in monodentate structures on defect-free anatase (101) at 300 K, 84-⁸⁶ and because monodentate species are expected to dominate to maximize the number of bound PhCOOH per unit area at high coverages, we propose that the monodentate structures are the most relevant ones to use in our designs of chemically responsive LCs. Furthermore, M1 becomes the energetically preferred structure on a (2x4) unit cell of anatase (101) (Figure S3); therefore, in the following we focus our DFT and molecular dynamics (MD) simulations on the M1 structure.

Table 1. Calculated binding and reaction energy (BE and ΔE , respectively) on clean anatase (101) for a (2x3) surface unit cell. Adsorption of H* and SO_x^* species are calculated to be coadsorbed on the same slab. All binding energies are calculated with one adsorbate on the slab. Most exothermic events are listed first.

	Equation	ΔE (eV)
R2	$SO_2(g) + 2H_2O(g) + 5* \rightarrow 4H^* + SO_4*$	-2.06
R1	$SO_2(g) + H_2O(g) + 3* \rightarrow 2H^* + SO_3*$	-1.79
BE _{PhCOOF}	$_{\rm H}$ PhCOOH(g) + * \rightarrow PhCOOH*	-1.32
$BE_{\rm H2O}$	$H_2O(g) + * \rightarrow H_2O*$	-0.96
$BE_{PhCN} \\$	$PhCN(g) + * \rightarrow PhCN*$	-0.74
BE _{SO2}	$SO_2(g) + * \rightarrow SO_2*$	-0.67

Significantly, the calculations reported above reveal that PhCOOH binds more strongly (by 0.36 eV) than H₂O to anatase (101) (Table 1), leading to the prediction that H₂O will not trigger changes in the orientation of PhCOOH-containing LCs on TiO₂, as required for water-tolerant responsive LCs.³⁷ In addition, because PhCOOH binds in a perpendicular orientation with a BE of -1.32 eV, we predict that PhCOOH-containing

LCs will adopt homeotropic anchoring on the clean anatase surfaces.

Guided by these computational predictions, we next performed experiments in which we measured the anchoring of CBCAcontaining LCs on anatase surfaces. Because CBCA is not mesogenic as a pure component at room temperature, we dissolved 0.005 mol% of CBCA into 5CB (CBCA-5CB (C_{CBCA}=0.005 mol%)) to create room-temperature-nematic mixtures (differential scanning calorimetry in SI confirmed that CBCA was well-mixed into 5CB). If we assume that all CBCA molecules in the 5CB partition to the anatase (101) surface due to CBCA's strong binding (BE = -1.32 eV, 0.58 eV stronger than PhCN), we calculate that 0.005 mol% CBCA in an 18 µmthick LC film will generate 0.39 ML CBCA coverage on the anatase (101) surface. Inspection of Figure 2d reveals that CBCA-5CB (C_{CBCA}=0.005 mol%) adopted a homeotropic orientation (dark image between crossed polarizers; Figure 2f) in experiments performed on the anatase surface under the ambient humidity (40±10% RH). This observation is consistent with computational predictions of strong binding of the PhCOOH group in CBCA to anatase (101) (-1.32 eV in Figure 1 and Table 1), stronger than both the PhCN group of the 5CB (-0.74 eV) and H₂O present in the ambient environment (-0.96 eV). Without CBCA, as reported earlier in this paper, 5CB does not assume a homeotropic orientation in the presence of 40±10% RH.

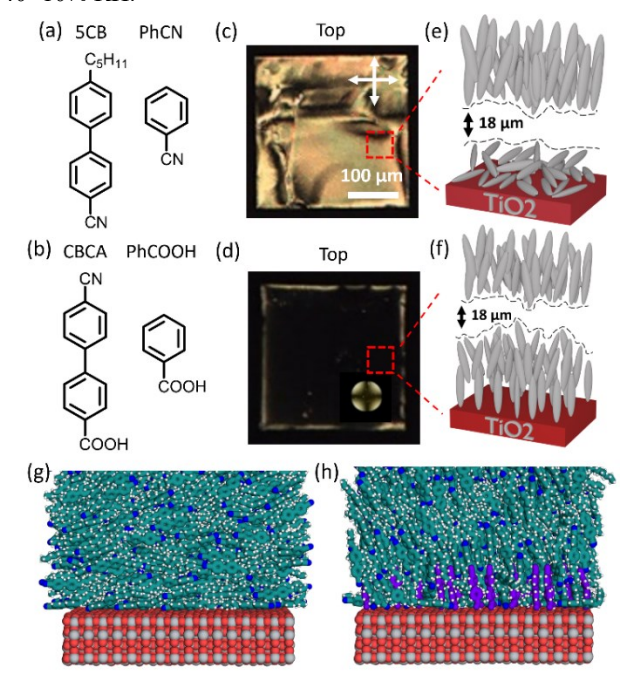


Figure 2. (a) Molecular structures of 5CB and its surrogate PhCN. (b) Molecular structures of CBCA and its surrogate PhCOOH. Optical images (crossed polarizers) of (c) 5CB and (d) CBCA-5CB ($C_{CBCA} = 0.005 \text{ mol}\%$) hosted in copper grids on $3.27\pm0.03 \text{ nm}$ -thick anatase TiO_2 in the ambient environment ($40\pm10\%$ RH). Schematic illustrations of the planar (e) and homeotropic (f) orientation of liquid crystals at LC-solid interfaces. Molecular dynamics simulations of (g) 5CB and (h) CBCA-5CB mixture on anatase (101) (the images are cropped; see full images in SI). Gray is titanium, red is oxygen, green+blue is 5CB (blue is nitrogen), and purple is CBCA.

To confirm that a coverage of 0.39 ML CBCA on anatase (101) is sufficient to cause homeotropic anchoring of a film of CBCA-5CB, we performed DFT energy-minimizing simulations to determine the structural and energetic parameters of the M1 structure for use in subsequent MD simulations (see SI for additional details). Figure 2g and Figure 2h show the resulting orientations predicted by MD simulations of the LC on the anatase (101) surface without and with 0.5 ML CBCA, respectively. These simulated structures, along with calculated long-range orientational order, as described by a scalar order parameter (P_2 order parameter, see details in SI) near the surface, further support that CBCA binding to the surface induces homeotropic anchoring of a CBCA-5CB film, as observed in experiments.

Ordering Transitions Triggered by Surface Reactions of SO₂

For the homeotropically oriented LC of CBCA and 5CB supported on anatase (101) to respond to the presence of SO_2 , SO_2 would have to bind on anatase (101) more strongly than the binding of PhCOOH to displace CBCA. To explore this possibility, we first calculated the BE of SO_2 (Table 1; structure in SI) to be -0.67 eV, which is weaker than the BE of PhCOOH to anatase (101) (-1.32 eV), predicting that CBCA will not be displaced by SO_2 . To test this computational prediction, $18 \, \mu m$ -thick LC films of CBCA-5CB ($C_{CBCA} = 0.005 \, mol\%$) were deposited onto anatase surfaces and subsequently exposed to a stream of dry N_2 containing $5\pm0.3 \, ppm \, SO_2$ (1000 mL/min). We observed the LC to maintain its perpendicular orientation during the 1 hour-exposure to the SO_2 (Figure S7b). This result is consistent with the computational prediction that dry SO_2 cannot displace CBCA from the surface of anatase (101).

Prior studies have reported the effects of H₂O (relative humidity) on the speciation of SO₂ adsorbed on anatase TiO₂ thin films and nanoparticles. 82,83,90 Specifically, SO₃- or/and SO₄-like adsorbate structures were found under humid conditions as characterized by IR^{83,90} or XPS.⁸² Motivated by these prior experimental studies, we computationally evaluated the surface reaction of adsorbed SO₂ and H₂O to form SO₃- or SO₄-like species on anatase (101) (Table 1). These computations led us to predict that adsorbed PhCOOH would be displaced on anatase (101) by either $2H^* + SO_3^*$ (-1.79 eV, Figure 1 and Figure 3b) or $4H^* + SO_4^*$ (-2.06 eV, Figure S21). Inspired by the prediction that the products of a reaction between H₂O and SO₂ on anatase (101) can generate surface species that displace adsorbed PhCOOH, we exposed CBCA-5CB mixtures supported on anatase surfaces to 2±0.1 ppm SO₂ at 40% RH. As shown in Figure 3c, we observed the LC to undergo a dynamic orientational transition that initiated approximately 100 seconds after the onset of exposure to SO₂ and H₂O. With increasing duration of exposure to humid SO₂, we observed an increase in the brightness of the LC, eventually leading to a uniformly bright LC film. The continuous change in interference colors observed during the exposure indicates the presence of a continuous LC anchoring transition (LC molecules are tilting). As a control experiment, we exposed the same LC system to a stream of N2 containing 40% RH for 1 hour. We observed the LCs to maintain their perpendicular orientation (Figure S7b), consistent with the computational prediction that H₂O cannot displace CBCA. These results, when combined, lead us to conclude that the SO₂ and H₂O mixture triggered the orientational response of the LC. In addition to evaluating the response of the LC to humid SO_2 at 40% RH, we also tested the response of the same LC mixture to 2 ± 0.1 ppm SO_2 at 20%, 60%, and 80% RH. We measured no significant influence of relative humidity on the dynamics of the LC response to SO_2 (Figure S8).

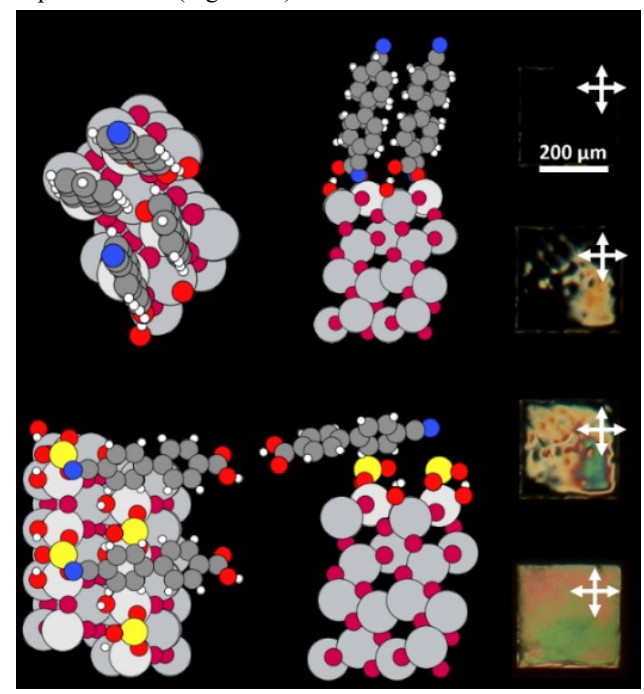


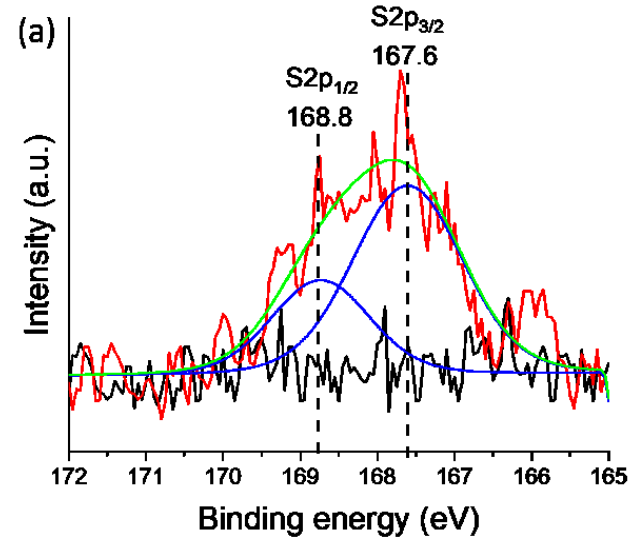
Figure 3. Top and cross-section view for the energetically preferred orientations of (a) 2 CBCA and 2 PhPhCN molecules on a (2x2) anatase (101) surface unit cell and (b) 2 CBCA molecules on $8H^* + 4SO_3^*$ -covered (2x4) anatase (101). (c) Optical responses (crossed polarizers) of CBCA-5CB (C_{CBCA} = 0.005 mol%) to 2 ± 0.1 ppm SO₂ with 40% RH at 0, 100, 140, and 200 seconds after onset of exposure.

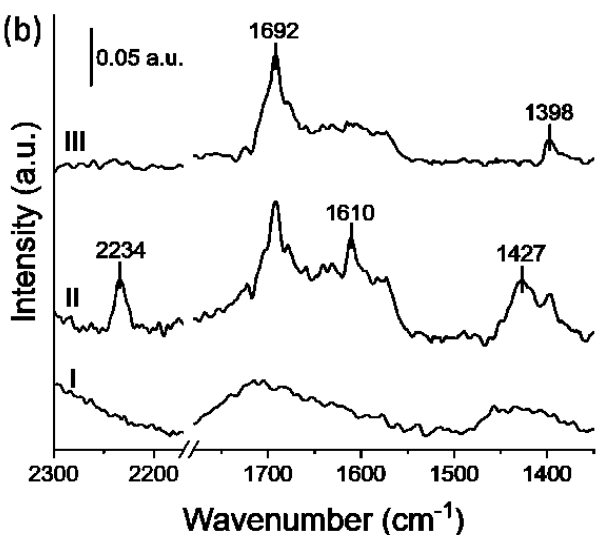
Binding of CBCA and SO₂ with Anatase (101)

To further understand the structure of the SO_2 - and H_2O -derived adsorbates on anatase (101) after exposure to humid SO_2 , we performed XPS measurements. The anatase surfaces were first coated with 18 µm-thick films of the CBCA-5CB mixture, exposed to 5 ppm SO_2 at 40% RH for 10 minutes, and then rinsed with ethanol to remove the LC prior to performing XPS. Inspection of Figure 4a reveals that, after exposure to humid SO_2 , a peak corresponding to S2p is clearly evident. The S2p peak can be deconvoluted into $S2p_{1/2}$ and $S2p_{3/2}$ peaks, which are used to determine the identity of the S-containing species. Phase $S2p_{3/2}$ binding energy at $S2p_{3/2}$ binding energ

The above-described experimental observation generates an unanswered question: why is the SO₄-like species not observed on the surface even if the formation of this species is thermodynamically favored over the SO₃-like species (Table 1)? To address this question, we computationally evaluated the kinetics of a reaction between SO₃* and H₂O to form SO₄* but found this to be kinetically infeasible at room temperature (Figure S17). SO₃ and H₂O both bind strongly, which means that there is a large energy cost to form the new bond in the SO₄ species. We computed the barrier of the most difficult

elementary step to be 2.06 eV, well above what is kinetically feasible at room temperature. This result is in agreement with the experiments where the SO₃-like, but not SO₄-like, species was observed in the XPS measurement.





(c) Assignment Measured Calculated frequency (cm-1) frequency (cm⁻¹) v(C≡N) 2234 2260 v(C=O) 1692 1659 v(C-C)_{ring} 1610 1608 $v(C-C)_{ring}$ 1427 1410 β(C-O-H) 1398 1347

Figure 4. (a) X-ray photoelectron spectroscopy (XPS) of the S2p region for anatase TiO₂ before (black) and after (red) exposure to 5 ppm SO₂ at 40% RH for 10 minutes. The spectral deconvolution (blue) of S2p to S2p_{1/2} at 168.8±0.1 eV and S2p_{3/2} at 167.6±0.2 eV, and their summation (green). (b) PM-IRRAS of anatase before exposure to CBCA and humid SO₂ (I) and nanometer-thick layers of CBCA on anatase (II), and humid SO₂-exposed anatase surfaces (III). (c) Vibrational frequency (cm⁻¹) assignments^{40,91,92} for peaks in (b). v represents stretching, and β represents in-plane bending.

Next, to confirm that the orientational transition of the CBCA-5CB LC triggered by humid SO₂ was caused by a change in the molecular interactions of CBCA and anatase (101), we performed polarization-modulation infrared reflectance absorbance spectroscopy (PM-IRRAS) of CBCA on anatase (101).65 We performed these measurements by spin-coating a thin film (ellipsometric thickness of ~2 nm) of CBCA onto anatase-coated Pt films (see detailed information in Methods). Inspection of the IR spectra shown in Figure 4b(II) and the assignments of IR peaks in Figure 4c reveals that the peaks corresponding to the nitrile group (2234 cm⁻¹), the carbonyl group (1692 cm⁻¹), and the benzene ring (1610 and 1427 cm⁻¹) are evident for CBCA. When combined with the surfaceselection rules for PM-IRRAS on anatase surfaces, 93 this observation indicates that these functional groups of CBCA have transition dipole moments that project onto the normal of the anatase surface. Moreover, we found the appearance of the C-O-H in-plane bending mode at 1398 cm⁻¹ (Figure 4b(II)), indicating no dissociation of COOH on anatase (101), consistent with prior experimental studies on formic acid adsorption on anatase (101) in a molecular monodentate geometry.84-86 This result is also consistent with the monodentate binding structure determined in our electronic structure calculations (see Figure 1) and used in our MD simulations, as discussed earlier.

We then used PM-IRRAS to characterize the influence of humid SO₂ exposure on the molecular interactions between CBCA and anatase. As shown in Figure 4b(III), the IR bands corresponding to the nitrile peak (2234 cm⁻¹) and C-C stretching peak (1610 and 1427 cm⁻¹), both of which are evident prior to the exposure to 5 ppm SO₂ at 40% RH, are not present after CBCA contacts the humid-SO₂-treated anatase surface. This result is consistent with our observations of a planar orientation of the CBCA-5CB film on the anatase surface after exposure to humid SO₂, as shown in Figure 3. Interestingly, we observed IR peaks associated with the carbonyl (1692 cm⁻¹) and hydroxyl (1398 cm⁻¹) groups but not the phenyl groups. This result is similar to the IR spectrum of CBCA in a parallel orientation on a Cl-covered Au (111) surface, in which the phenyl rings adopt a parallel orientation on the surface and the carboxylic group plane rotates relative to the phenyl ring of CBCA with the lowest free energy.⁴⁰ To explore this orientation, we calculated an energy-minimized stable structure showing the rotation of the COOH group relative to the surface in Figure 3b. In this structure, the COOH is rotated 45° (defined as the angle between the O-C-O plane relative to the surface normal), which means that the absorbance corresponding to the C=O would be observable due to the surface-selection rule. Overall, these experiments provide additional support for our conclusion that the orientational response observed in Figure 3 is due to the change of the orientation of CBCA molecules at the surface of anatase (101) after exposure to humid SO₂.

Chemical Selectivity

The computational and experimental results presented above support our conclusion that humid SO_2 can trigger CBCA-5CB mixtures to undergo orientational transitions on anatase surfaces due to the more negative reaction energy, ΔE (-1.79 eV in Table 1) of the SO_2 + H_2O surface reaction (R1) as compared to the BE of CBCA (-1.32 eV). Here, we predict the chemical selectivity of LCs using a strategy of comparing our calculated reaction/binding energies of chemical species (ΔE) with the

binding energy of CBCA (BE_{PhCOOH}) on anatase (101) (Table S3 and Figure 5a). Specifically, if the displacement energy ($D_{\Delta E}$) calculated from the difference in ΔE and BE_{PhCOOH} is negative, then we predict the LC response to be thermodynamically favorable.³⁸

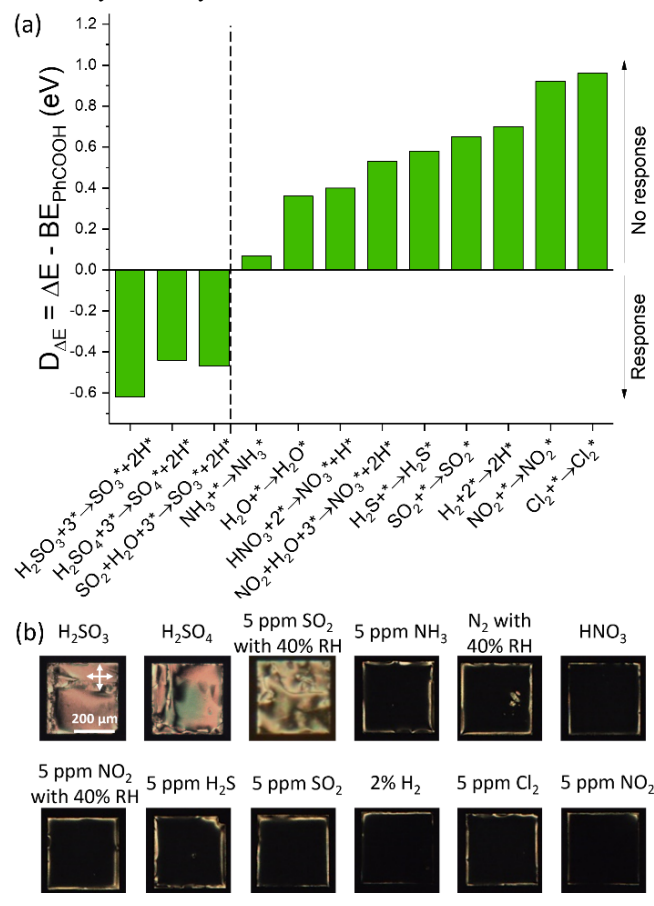


Figure 5. (a) Comparison of experimental responses of CBCA-5CB (C_{CBCA} = 0.005 mol%) on anatase surfaces to different chemical species and calculated displacement energy DAE for PhCOOH on a (2x3) unit cell of anatase (101) for the events listed in the x-axis. A response is predicted to occur when the $D_{\Delta E}$ is negative. Green color of the bars represents the agreement between theoretical predictions and experimental observations. We find agreement for each case between theory and experiment. (b) Optical images (crossed polarizers) of CBCA-5CB (C_{CBCA} = 0.005 mol%) hosted in copper grids on anatase surfaces after exposure to 5 ppm NH₃, N₂ at 40% RH, 5 ppm NO₂ at 40% RH, 5 ppm H₂S, 5 ppm SO₂, 2% H₂, 5 ppm Cl₂ and 5 ppm NO₂ for 1 hour, and 5 ppm SO₂ at 40% RH for 5 mins. For H₂SO₃, H₂SO₄, and HNO₃, prior to the deposition of LC on anatase surfaces, the surfaces were first dipped in their solutions with 0.1 M concentration for 1 hour, then rinsed with copious amounts of deionized water, and dried under a stream of nitrogen.

The values of $D_{\Delta E}$ in Figure 5a were calculated from DFT and the values of ΔE are reported in Table S3 and respective structures are shown in Figure S22. Inspection of Figure 5a reveals that the adsorption of H_2SO_3 and H_2SO_4 , and the reaction of SO_2 with H_2O , have negative values of $D_{\Delta E}$, predicting a response in the CBCA-5CB mixture upon exposure to $H_2SO_3,\,H_2SO_4,$ or humid SO_2 (already discussed above). To test the predicted response to H_2SO_3 and H_2SO_4 experimentally, prior to the deposition of LC on anatase surfaces, we exposed

anatase surfaces to solutions of 0.1 M H₂SO₃ or H₂SO₄ for 1 hour, then rinsed with copious amounts of deionized water, and dried under a stream of nitrogen. Figure 5b shows that the CBCA-5CB mixture adopted a planar orientation on the H₂SO₃ or H₂SO₄-treated anatase surface. This observation and the response to humid SO₂ discussed earlier are consistent with the computational prediction of negative $D_{\Delta E}$ (indicated by the green color in Figure 5a). Similarly, we also calculated the $D_{\Delta E}$ of CBCA by other chemical species (NH3, H2O, HNO3, NO₂+H₂O, H₂S, SO₂, H₂, NO₂, and Cl₂) and found that they are all positive, leading us to predict no response upon exposure to them. We conducted experiments using all the chemical species addressed using DFT and the results are summarized in Figure 5b. The experimental observations are in good agreement with our predictions (indicated by the green color in Figure 5a). Overall, these results demonstrate that electronic structure calculations of D_{AE} can be combined with experiments to design a LC system of CBCA-5CB on anatase (101) that provides high selectivity to SO₂ over other chemical species.

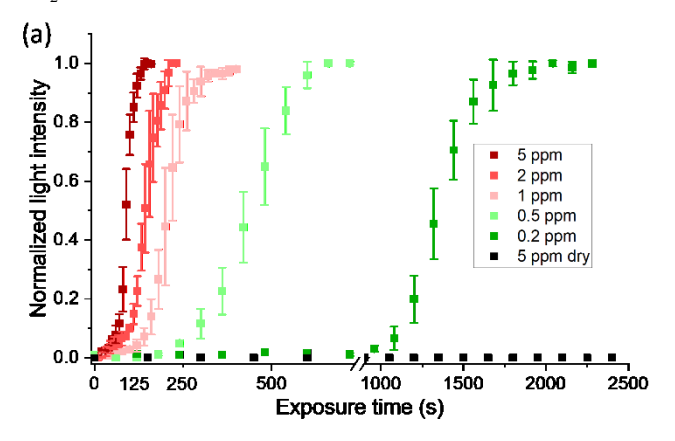
Dependence of LC Dynamics on Concentration of SO₂

We characterized the dynamic response of the CBCA-5CB LC supported on anatase (101) to decreasing concentrations of SO_2 (5 ± 0.3 , 2 ± 0.1 , 1 ± 0.06 , 0.5 ± 0.03 , and 0.2 ± 0.01 ppm) at 40% RH. Inspection of Figure 6a reveals slower LC responses to lower SO_2 concentrations. These results are significant because the time-dependent response of the LC shown in Figure 6a can be analyzed using a simple transport-reaction model (with transport parameters calculated from MD simulation; see SI) to provide insight into the interfacial processes that control the dynamic response of the LC. As detailed in SI, this analysis revealed that the dynamic response of the LC to humid SO_2 is not limited by the surface reaction kinetics (they are fast) but rather rate-limited by diffusion of SO_2 to the LC-metal oxide interface (Table S1 and S2).

To provide additional evidence that the LC response to SO₂ on anatase (101) is not reaction-limited, we performed climbing image nudged elastic band calculations⁹⁵ to obtain activation energy barriers for reaction pathways between SO₂ and H₂O. Detailed descriptions of these calculations along with potential energy diagrams and relevant structures can be found in SI; here we present the main conclusions from these computations. First, we found that the anatase (101) surface is required to lower the activation energy barrier for the reaction between SO₂ and H₂O sufficiently to allow the reaction to occur at room temperature (reaction in the LC or gas phase is unlikely to occur at room temperature). Second, we found that H₂O adsorbs molecularly, in agreement with experimental and DFT studies, 96,97 but can dissociate with a barrier of only 0.27 eV (Figure S15). We also found that SO₂ can react with dissociated H₂O without a barrier to form SO₃H* + H*. This prediction agrees with the conclusions of our analysis of our transportreaction model (fast reaction). Finally, we comment that Figure S15 shows a pathway that yields SO₃* from SO₃H* with a barrier of only 0.41 eV, indicating that this reaction could occur at room temperature.

As noted above, the largest anthropogenic source of SO₂ in the atmosphere is the burning of sulfur-containing fossil fuels for domestic heating, power generation, and motor vehicles. The US Environmental Protection Agency (EPA) specifies that the atmospheric concentration of SO₂ (averaged over 1-hour) should not exceed 75 ppb. 98 Although mixtures of CBCA-5CB

 $(C_{CBCA} = 0.005 \text{ or } 0.001 \text{ mol}\%)$ supported on anatase (101) did not respond to 75 ppb SO₂ (Figure 6c), we found it was possible to design a LC system with sensitivity to 75 ppb of SO₂ by using CBCA dissolved in a mixture of 65 mol% 4-(trans-4'pentylcyclohexyl)-benzonitrile (PCH5) and 35 mol% 4-(trans-4'-propylcyclohexyl)-benzonitrile (PCH3) (Figure 6b), which forms a nematic LC phase at room temperature. 63 This choice of LC was informed by our prior finding that the tilted/planar anchoring of PCH at free surfaces (LC-air interface) leads to a faster response and greater sensitivity of the LC to targeted chemical species as compared to 5CB (due to a release of elastic energy stored in the initial, strained state of the LC (Figure S13)).⁶³ Overall, this result reveals that LC systems supported on anatase (101) can be sufficiently sensitive to SO₂ that they offer fresh approaches for environmental monitoring of SO₂ concentrations. SO₂ concentrations involved in human exposure standards are typically higher than atmospheric (the US Occupational Safety and Health standards Administration limits personal exposure to SO₂ to 5 ppm for 15 mins and 2 ppm SO₂ over 8 hours²⁴), and thus we conclude that the LC response to SO₂ on TiO₂ is promising also for use in wearable dosimeters that measure cumulative exposure to SO_{2} .99



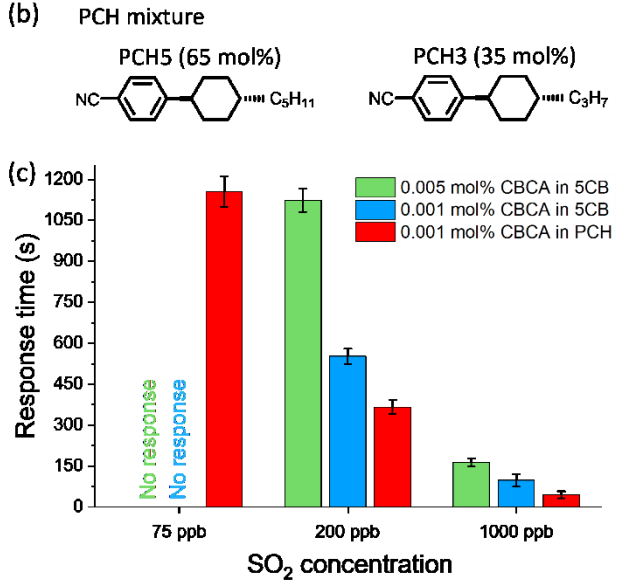


Figure 6. (a) Normalized intensity of polarized light transmitted through CBCA-5CB ($C_{CBCA} = 0.005 \text{ mol}\%$) supported on anatase surfaces during the exposure to 5±0.3, 2±0.1, 1±0.06, 0.5±0.03, 0.2±0.01 ppm SO₂ at 40% RH, and 5±0.3 ppm dry SO₂. (b) Molecular structures of PCH5 and PCH3. The PCH mixture

contained 65 mol% PCH5 and 35 mol% PCH3.⁶³ (c) Response time of three LC systems following exposure to 75±5, 200±10, or 1000±60 ppb SO₂ gas at 40% RH. The response time is defined as the interval of time between the introduction of SO₂ and the measurement of a 10% change in optical retardance of the LC film.

CONCLUSIONS

In summary, we have demonstrated that it is possible to couple the catalytic activity of metal oxide surfaces with sulfur oxide species to ordering transitions in LCs. The ordering transitions of the LC provide a facile means of amplifying reactions of relevance to atmospheric chemistry into the optical scale. More broadly, the results are conceptually important because they demonstrate that it is possible to leverage first-principles insights from computational methods and the rich literature of surface science, heterogeneous catalysis on metal oxides and atmospheric chemistry to design both equilibrium and dynamic properties of chemically responsive materials. We combined electronic structure calculations, molecular dynamic simulations, and experiments to show that CBCA binds to anatase (101) when doped into nematic 5CB and thereby causes the LC host to adopt a homeotropic orientation. Furthermore, we demonstrated that CBCA bound to anatase is displaced by SO₃-like species, the product of a surface-catalyzed reaction of SO₂ with H₂O, as confirmed by XPS and PM-IRRAS, and that the displacement triggers a change in orientation of the LC film. The response is highly selective to humid SO₂ over other gases, in agreement with our computational chemistry predictions. Lastly, by using a LC formed of CBCA and PCH, we show that the LC system can respond to gas phase SO₂ concentrations as low as 75 ppb. The dynamic response of the LC system is mass transport limited, suggesting that higher sensitivity and faster dynamic responses can be engineered by optimizing the gas flow to the LC system (the response is not limited by the intrinsic kinetics of the SO₂ reaction on the anatase (101) surface). Overall, the results in this paper enable a range of future directions of research including the design of LCs that respond to the photocatalytic properties of titanium dioxide^{32,55} or catalytic reactions of relevance to atmospheric chemistry occurring on other metal oxides, such as tin oxide⁵³ and zinc oxide.54

ASSOCIATED CONTENT

Supporting Information. The Supporting Information is available free of charge via the Internet at http://pubs.acs.org.

Characterization of surfaces; additional simulation details; optical images; discussion of transport model, potential energy diagrams and selectivity (PDF)

AUTHOR INFORMATION

Corresponding Author

*emavrikakis@wisc.edu (Manos Mavrikakis)

*nla34@cornell.edu (Nicholas L. Abbott)

Author Contributions

‡N.B. and J.I.G. contributed equally to this work.

Notes

N.L.A. declares a financial interest in Platypus Technologies LLC,

a for-profit company that has developed LC-based analytic technologies.

ACKNOWLEDGMENT

We acknowledge financial support from the US National Science Foundation under grants IIS-1837812 and 1837821. This work was performed in part at the Cornell NanoScale Facility, a member of the National Nanotechnology Coordinated Infrastructure (NNCI), which is supported by the National Science Foundation (Grant NNCI-2025233). This work was also partially supported by the Cornell Center for Materials Research with funding from the NSF MRSEC program (DMR-1719875).

REFERENCES

- H.-J. Schneider. Chemoresponsive Materials; RSC Smart Materials: London, 2015.
- (2) Paxton, W. F.; Kistler, K. C.; Olmeda, C. C.; Sen, A.; St. Angelo, S. K.; Cao, Y.; Mallouk, T. E.; Lammert, P. E.; Crespi, V. H. Catalytic Nanomotors: Autonomous Movement of Striped Nanorods. J. Am. Chem. Soc. 2004, 126 (41), 13424–13431.
- (3) Hu, J.; Liu, S. Responsive Polymers for Detection and Sensing Applications: Current Status and Future Developments. *Macromolecules* 2010, 43 (20), 8315–8330.
- (4) Mohapatra, H.; Kim, H.; Phillips, S. T. Stimuli-Responsive Polymer Film That Autonomously Translates a Molecular Detection Event into a Macroscopic Change in Its Optical Properties via a Continuous, Thiol-Mediated Self-Propagating Reaction. J. Am. Chem. Soc. 2015, 137 (39), 12498–12501.
- (5) Parmar, J.; Vilela, D.; Villa, K.; Wang, J.; Sánchez, S. Microand Nanomotors as Active Environmental Microcleaners and Sensors. J. Am. Chem. Soc. 2018, 140 (30), 9317–9331.
- (6) Walther, A. Viewpoint: From Responsive to Adaptive and Interactive Materials and Materials Systems: A Roadmap. Adv. Mater. 2020, 32 (20), 1905111.
- (7) Chen, J. K.; Chang, C. J. Fabrications and Applications of Stimulus-Responsive Polymer Films and Patterns on Surfaces: A Review. *Materials (Basel)*. 2014, 7 (2), 805–875.
- (8) Gomes, B. S.; Simões, B.; Mendes, P. M. The Increasing Dynamic, Functional Complexity of Bio-Interface Materials. *Nat. Rev. Chem.* 2018, 2 (3), 0120.
- (9) Mirvakili, S. M.; Hunter, I. W. Artificial Muscles: Mechanisms, Applications, and Challenges. Adv. Mater. 2018, 30 (6), 1–28.
- (10) McCune, J. A.; Mommer, S.; Parkins, C. C.; Scherman, O. A. Design Principles for Aqueous Interactive Materials: Lessons from Small Molecules and Stimuli-Responsive Systems. Adv. Mater. 2020, 32, 1906890.
- (11) Su, B.; Tian, Y.; Jiang, L. Bioinspired Interfaces with Superwettability: From Materials to Chemistry. *J. Am. Chem. Soc.* **2016**, *138* (6), 1727–1748.
- (12) Blum, A. P.; Kammeyer, J. K.; Rush, A. M.; Callmann, C. E.; Hahn, M. E.; Gianneschi, N. C. Stimuli-Responsive Nanomaterials for Biomedical Applications. *J. Am. Chem. Soc.* 2015, 137 (6), 2140–2154.
- (13) Reinitzer, F. Beiträge Zur Kenntniss Des Cholesterins. *Monatshefte für Chemie* **1888**, *9*, 421–441.
- (14) Yokoyama, H. Surface Anchoring of Nematic Liquid Crystals. Mol. Cryst. Liq. Cryst. Inc. Nonlinear Opt. 1988, 165, 265–361.
- (15) Jerome, B. Surface Effects and Anchoring in Liquid Crystals. Reports Prog. Phys. 1991, 54, 391–451.
- (16) Drzaic, P. S. *Liquid Crystal Dispersions*; World Scientific, 1995
- (17) Govindaraju, T.; Bertics, P. J.; Raines, R. T.; Abbott, N. L. Using Measurements of Anchoring Energies of Liquid Crystals on Surfaces to Quantify Proteins Captured by Immobilized Ligands. J. Am. Chem. Soc. 2007, 129, 11223–11231.
- (18) Tsuei, M.; Shivrayan, M.; Kim, Y.-K.; Thayumanavan, S.; Abbott, N. L. Optical "Blinking" Triggered by Collisions of Single Supramolecular Assemblies of Amphiphilic Molecules with Interfaces of Liquid Crystals. J. Am. Chem. Soc. 2020, 142

- (13), 6139–6148.
- (19) Concellón, A.; Fong, D.; Swager, T. M. Complex Liquid Crystal Emulsions for Biosensing. *J. Am. Chem. Soc.* **2021**, *143* (24), 9177–9182.
- (20) Schwartz, J. J.; Mendoza, A. M.; Wattanatorn, N.; Zhao, Y.; Nguyen, V. T.; Spokoyny, A. M.; Mirkin, C. A.; Baše, T.; Weiss, P. S. Surface Dipole Control of Liquid Crystal Alignment. J. Am. Chem. Soc. 2016, 138 (18), 5957–5967.
- (21) Concellón, A.; Zentner, C. A.; Swager, T. M. Dynamic Complex Liquid Crystal Emulsions. J. Am. Chem. Soc. 2019, 141 (45), 18246–18255.
- (22) Bukusoglu, E.; Pantoja, M. B.; Mushenheim, P. C.; Wang, X.; Abbott, N. L. Design of Responsive and Active (Soft) Materials Using Liquid Crystals. Annu. Rev. Chem. Biomol. Eng. 2016, 7, 163–196
- (23) Forbes, P. Atmospheric Chemistry Analysis: A Review. Anal. Chem. 2020, 92 (1), 455–472.
- (24) Occupational Safety and Health Administration. https://www.osha.gov/annotated-pels/table-z-1.
- (25) Hallquist, M.; Wenger, J. C.; Baltensperger, U.; Rudich, Y.; Simpson, D.; Claeys, M.; Dommen, J.; Donahue, N. M.; George, C.; Goldstein, A. H.; Hamilton, J. F.; Herrmann, H.; Hoffmann, T.; Iinuma, Y.; Jang, M.; Jenkin, M. E.; Jimenez, J. L.; Kiendler-Scharr, A.; Maenhaut, W.; McFiggans, G.; Mentel, T. F.; Monod, A.; Prévôt, A. S. H.; Seinfeld, J. H.; Surratt, J. D.; Szmigielski, R.; Wildt, J. The Formation, Properties and Impact of Secondary Organic Aerosol: Current and Emerging Issues. Atmos. Chem. Phys. 2009, 9 (14), 5155–5236.
- (26) Kiehl, J. T.; Briegleb, B. P. The Relative Roles of Sulfate Aerosols and Greenhouse Gases in Climate Forcing. Science 1993, 260 (5106), 311–314.
- (27) Long, B.; Bao, J. L.; Truhlar, D. G. Reaction of SO₂ with OH in the Atmosphere. *Phys. Chem. Chem. Phys.* **2017**, *19* (11), 8091– 8100
- (28) Liu, T.; Chan, A. W. H.; Abbatt, J. P. D. Multiphase Oxidation of Sulfur Dioxide in Aerosol Particles: Implications for Sulfate Formation in Polluted Environments. *Environ. Sci. Technol.* 2021, 55 (8), 4227–4242.
- (29) Zhong, J.; Zhu, C.; Li, L.; Richmond, G. L.; Francisco, J. S.; Zeng, X. C. Interaction of SO₂ with the Surface of a Water Nanodroplet. J. Am. Chem. Soc. 2017, 139 (47), 17168–17174.
- (30) Park, J.; Jang, M.; Yu, Z. Heterogeneous Photo-Oxidation of SO₂ in the Presence of Two Different Mineral Dust Particles: Gobi and Arizona Dust. *Environ. Sci. Technol.* 2017, 51 (17), 9605–9613.
- (31) He, H.; Wang, Y.; Ma, Q.; Ma, J.; Chu, B.; Ji, D.; Tang, G.; Liu, C.; Zhang, H.; Hao, J. Mineral Dust and NO_x Promote the Conversion of SO₂ to Sulfate in Heavy Pollution Days. Sci. Rep. 2014, 4 (1), 4172.
- (32) Chen, H.; Nanayakkara, C. E.; Grassian, V. H. Titanium Dioxide Photocatalysis in Atmospheric Chemistry. *Chem. Rev.* 2012, 112 (11), 5919–5948.
- (33) White, T. J.; McConney, M. E.; Bunning, T. J. Dynamic Color in Stimuli-Responsive Cholesteric Liquid Crystals. *J. Mater.* Chem. 2010, 20 (44), 9832.
- (34) Sutarlie, L.; Qin, H.; Yang, K.-L. Polymer Stabilized Cholesteric Liquid Crystal Arrays for Detecting Vaporous Amines. *Analyst* **2010**, *135* (7), 1691.
- (35) Shah, R. R.; Abbott, N. L. Principles for Measurement of Chemical Exposure Based on Recognition-Driven Anchoring Transitions in Liquid Crystals. *Science* 2001, 293 (5533), 1296– 1299.
- (36) Roling, L. T.; Scaranto, J.; Herron, J. A.; Yu, H.; Choi, S.; Abbott, N. L.; Mavrikakis, M. Towards First-Principles Molecular Design of Liquid Crystal-Based Chemoresponsive Systems. *Nat. Commun.* 2016, 7, 13338.
- (37) Yu, H.; Szilvási, T.; Rai, P.; Twieg, R. J.; Mavrikakis, M.; Abbott, N. L. Computational Chemistry-Guided Design of Selective Chemoresponsive Liquid Crystals Using Pyridine and Pyrimidine Functional Groups. Adv. Funct. Mater. 2018, 28 (13), 1703581.
- (38) Szilvási, T.; Bao, N.; Yu, H.; Twieg, R. J.; Mavrikakis, M.; Abbott, N. L. The Role of Anions in Adsorbate-Induced Anchoring Transitions of Liquid Crystals on Surfaces with Discrete Cation Binding Sites. Soft Matter 2018, 14 (5), 797–

- 805.
- (39) Yang, K.; Cadwell, K.; Abbott, N. L. Mechanistic Study of the Anchoring Behavior of Liquid Crystals Supported on Metal Salts and Their Orientational Responses to Dimethyl Methylphosphonate. J. Phys. Chem. B 2004, 108 (52), 20180– 20186
- (40) Yu, H.; Szilvási, T.; Wang, K.; Gold, J. I.; Bao, N.; Twieg, R. J.; Mavrikakis, M.; Abbott, N. L. Amplification of Elementary Surface Reaction Steps on Transition Metal Surfaces Using Liquid Crystals: Dissociative Adsorption and Dehydrogenation. J. Am. Chem. Soc. 2019, 141 (40), 16003–16013.
- (41) Szilvási, T.; Yu, H.; Gold, J. I.; Bao, N.; Wolter, T. J.; Twieg, R. J.; Abbott, N. L.; Mavrikakis, M. Coupling the Chemical Reactivity of Bimetallic Surfaces to the Orientations of Liquid Crystals. *Mater. Horizons* 2021, 8 (7), 2050–2056.
- (42) Chang, C.-K.; Kuo, H.-L.; Tang, K.-T.; Chiu, S.-W. Optical Detection of Organic Vapors Using Cholesteric Liquid Crystals. Appl. Phys. Lett. 2011, 99 (7), 073504.
- (43) Saha, A.; Tanaka, Y.; Han, Y.; Bastiaansen, C. M. W.; Broer, D. J.; Sijbesma, R. P. Irreversible Visual Sensing of Humidity Using a Cholesteric Liquid Crystal. *Chem. Commun.* 2012, 48 (38), 4579.
- (44) Su, X.; Voskian, S.; Hughes, R. P.; Aprahamian, I. Manipulating Liquid-Crystal Properties Using a PH Activated Hydrazone Switch. *Angew. Chemie Int. Ed.* 2013, 52 (41), 10734–10739.
- (45) Cachelin, P.; Green, J. P.; Peijs, T.; Heeney, M.; Bastiaansen, C. W. M. Optical Acetone Vapor Sensors Based on Chiral Nematic Liquid Crystals and Reactive Chiral Dopants. Adv. Opt. Mater. 2016, 4 (4), 592–596.
- (46) Yang, Y.; Kim, Y.-K.; Wang, X.; Tsuei, M.; Abbott, N. L. Structural and Optical Response of Polymer-Stabilized Blue Phase Liquid Crystal Films to Volatile Organic Compounds. ACS Appl. Mater. Interfaces 2020, 12 (37), 42099–42108.
- (47) Pschyklenk, L.; Wagner, T.; Lorenz, A.; Kaul, P. Optical Gas Sensing with Encapsulated Chiral-Nematic Liquid Crystals. ACS Appl. Polym. Mater. 2020, 2 (5), 1925–1932.
- (48) Esteves, C.; Ramou, E.; Porteira, A. R. P.; Moura Barbosa, A. J.; Roque, A. C. A. Seeing the Unseen: The Role of Liquid Crystals in Gas-Sensing Technologies. *Adv. Opt. Mater.* 2020, 8 (11), 1902117.
- (49) Schelski, K.; Reyes, C. G.; Pschyklenk, L.; Kaul, P.-M.; Lagerwall, J. P. F. Quantitative Volatile Organic Compound Sensing with Liquid Crystal Core Fibers. *Cell Reports Phys. Sci.* 2021, 100661
- (50) Henrich, Victor E.; Cox, P. A. The Surface Science of Metal Oxides, 1996th ed.; Cambridge University Press.
- (51) Diebold, U.; Li, S. C.; Schmid, M. Oxide Surface Science. Annu. Rev. Phys. Chem. 2010, 61, 129–148.
- (52) Védrine, J. C. Heterogeneous Catalysis on Metal Oxides. *Catalysts* **2017**, *7* (11), 341.
- (53) Batzill, M.; Diebold, U. The Surface and Materials Science of Tin Oxide. Prog. Surf. Sci. 2005, 79 (2–4), 47–154.
- (54) Wöll, C. The Chemistry and Physics of Zinc Oxide Surfaces. Prog. Surf. Sci. 2007, 82 (2–3), 55–120.
- (55) Schneider, J.; Matsuoka, M.; Takeuchi, M.; Zhang, J.; Horiuchi, Y.; Anpo, M.; Bahnemann, D. W. Understanding TiO₂ Photocatalysis: Mechanisms and Materials. *Chem. Rev.* 2014, 114 (19), 9919–9986.
- (56) Diebold, U. The Surface Science of Titanium Dioxide. Surf. Sci. Rep. 2003, 48 (5–8), 53–229.
- (57) Bai, J.; Zhou, B. Titanium Dioxide Nanomaterials for Sensor Applications. Chem. Rev. 2014, 114 (19), 10131–10176.
- (58) Weng, Z.; Guo, H.; Liu, X.; Wu, S.; Yeung, K. W. K.; Chu, P. K. Nanostructured TiO₂ for Energy Conversion and Storage. RSC Adv. 2013, 3 (47), 24758–24775.
- (59) Roscioni, O. M.; Muccioli, L.; Della Valle, R. G.; Pizzirusso, A.; Ricci, M.; Zannoni, C. Predicting the Anchoring of Liquid Crystals at a Solid Surface: 5-Cyanobiphenyl on Cristobalite and Glassy Silica Surfaces of Increasing Roughness. *Langmuir* 2013, 29 (28), 8950–8958.
- (60) Xia, Y.; Serra, F.; Kamien, R. D.; Stebe, K. J.; Yang, S. Direct Mapping of Local Director Field of Nematic Liquid Crystals at the Nanoscale. *Proc. Natl. Acad. Sci.* 2015, 112 (50), 15291– 15296
- (61) Choi, G. J.; Ryu, D. G.; Gwag, J. S.; Choi, Y.; Kim, T. H.; Park,

- M. S.; Park, I.; Lee, J. W.; Park, J. G. Anchoring Strength of Indium Tin Oxide Electrode Used as Liquid Crystal Alignment Layer. *J. Appl. Phys.* **2019**, *125* (6), 064501.
- (62) Klemas, V. V. Coastal and Environmental Remote Sensing from Unmanned Aerial Vehicles: An Overview. J. Coast. Res. 2015, 31, 1260–1267.
- (63) Nayani, K.; Rai, P.; Bao, N.; Yu, H.; Mavrikakis, M.; Twieg, R. J.; Abbott, N. L. Liquid Crystals with Interfacial Ordering That Enhances Responsiveness to Chemical Targets. Adv. Mater. 2018, 30 (27), 1706707.
- (64) Baer, D. R.; Artyushkova, K.; Cohen, H.; Easton, C. D.; Engelhard, M.; Gengenbach, T. R.; Greczynski, G.; Mack, P.; Morgan, D. J.; Roberts, A. XPS Guide: Charge Neutralization and Binding Energy Referencing for Insulating Samples. J. Vac. Sci. Technol. A 2020, 38 (3), 031204.
- (65) Buffeteau, T.; Desbat, B.; Turlet, J. M. Polarization Modulation FT-IR Spectroscopy of Surfaces and Ultra-Thin Films: Experimental Procedure and Quantitative Analysis. *Appl. Spectrosc.* 1991, 45 (3), 380–389.
- (66) Hunter, J. T.; Abbott, N. L. Dynamics of the Chemo-Optical Response of Supported Films of Nematic Liquid Crystals. Sensors Actuators, B Chem. 2013, 183, 71–80.
- (67) Kresse, G.; Furthmüller, J. Efficiency of Ab-Initio Total Energy Calculations for Metals and Semiconductors Using a Plane-Wave Basis Set. Comput. Mater. Sci. 1996, 6 (1), 15–50.
- (68) Kresse, G.; Furthmüller, J. Efficient Iterative Schemes for Ab Initio Total-Energy Calculations Using a Plane-Wave Basis Set. Phys. Rev. B - Condens. Matter Mater. Phys. 1996, 54 (16), 11169–11186.
- (69) Blöchl, P. E. Projector Augmented-Wave Method. Phys. Rev. B 1994, 50 (24), 17953–17979.
- (70) Joubert, D. From Ultrasoft Pseudopotentials to the Projector Augmented-Wave Method. *Phys. Rev. B - Condens. Matter Mater. Phys.* 1999, 59 (3), 1758–1775.
- (71) Perdew, J. P.; Burke, K.; Ernzerhof, M. Generalized Gradient Approximation Made Simple. *Phys. Rev. Lett.* 1996, 77 (18), 3865–3868.
- (72) Grimme, S.; Antony, J.; Ehrlich, S.; Krieg, H. A Consistent and Accurate Ab Initio Parametrization of Density Functional Dispersion Correction (DFT-D) for the 94 Elements H-Pu. J. Chem. Phys. 2010, 132 (15), 154104.
- (73) Pack, J. D.; Monkhorst, H. J. Special Points for Brillouin-Zone Integrations. *Phys. Rev. B* **1977**, *16* (4), 1748–1749.
- (74) Neugebauer, J.; Scheffler, M. Adsorbate-Substrate and Adsorbate-Adsorbate Interactions of Na and K Adlayers on Al(111). Phys. Rev. B 1992, 46 (24), 16067–16080.
- (75) Horn, M.; Schwebdtfeger, C. F.; Meagher, E. P. Refinement of the Structure of Anatase at Several Temperatures. *Zeitschrift für Krist. - Cryst. Mater.* 1972, 136 (1–6), 273–281.
- (76) Sheavly, J. K.; Gold, J. I.; Mavrikakis, M.; Van Lehn, R. C. Molecular Simulations of Analyte Partitioning and Diffusion in Liquid Crystal Sensors. *Mol. Syst. Des. Eng.* 2020, 5 (1), 304– 316.
- (77) Wang, J.; Wolf, R. M.; Caldwell, J. W.; Kollman, P. A.; Case, D. A. Development and Testing of a General Amber Force Field. J. Comput. Chem. 2004, 25 (9), 1157–1174.
- (78) Brandt, E. G.; Lyubartsev, A. P. Systematic Optimization of a Force Field for Classical Simulations of TiO₂-Water Interfaces. *J. Phys. Chem. C* 2015, 119 (32), 18110–18125.
- (79) Abraham, M. J.; Murtola, T.; Schulz, R.; Páll, S.; Smith, J. C.; Hess, B.; Lindah, E. Gromacs: High Performance Molecular Simulations through Multi-Level Parallelism from Laptops to Supercomputers. *SoftwareX* **2015**, *I*–2, 19–25.
- (80) Bakri, A. S.; Sahdan, M. Z.; Adriyanto, F.; Raship, N. A.; Said, N. D. M.; Abdullah, S. A.; Rahim, M. S. Effect of Annealing Temperature of Titanium Dioxide Thin Films on Structural and Electrical Properties. AIP Conf. Proc. 2017, 1788, 030030.
- (81) Zhang, X.; Zhuang, G.; Chen, J.; Wang, Y.; Wang, X.; An, Z.; Zhang, P. Heterogeneous Reactions of Sulfur Dioxide on Typical Mineral Particles. J. Phys. Chem. B 2006, 110, 12588– 12596.
- (82) Baltrusaitis, J.; Jayaweera, P. M.; Grassian, V. H. Sulfur Dioxide Adsorption on TiO₂ Nanoparticles: Influence of Particle Size, Coadsorbates, Sample Pretreatment, and Light on Surface Speciation and Surface Coverage. J. Phys. Chem. C 2011, 115

- (2), 492–500.
- (83) Nanayakkara, C. E.; Larish, W. A.; Grassian, V. H. Titanium Dioxide Nanoparticle Surface Reactivity with Atmospheric Gases, CO₂, SO₂, and NO₂: Roles of Surface Hydroxyl Groups and Adsorbed Water in the Formation and Stability of Adsorbed Products. J. Phys. Chem. C 2014, 118 (40), 23011–23021.
- (84) Xu, M.; Noei, H.; Buchholz, M.; Muhler, M.; Wöll, C.; Wang, Y. Dissociation of Formic Acid on Anatase TiO₂(101) Probed by Vibrational Spectroscopy. *Catal. Today* **2012**, *182* (1), 12–15
- (85) Kwon, S.; Lin, T. C.; Iglesia, E. Elementary Steps and Site Requirements in Formic Acid Dehydration Reactions on Anatase and Rutile TiO₂ Surfaces. J. Catal. 2020, 383, 60–76.
- (86) Tabacchi, G.; Fabbiani, M.; Mino, L.; Martra, G.; Fois, E. The Case of Formic Acid on Anatase TiO₂(101): Where Is the Acid Proton? Angew. Chemie - Int. Ed. 2019, 58 (36), 12431–12434.
- (87) Vittadini, A.; Selloni, A.; Rotzinger, F. P.; Grätzel, M. Formic Acid Adsorption on Dry and Hydrated TiO₂ Anatase (101) Surfaces by DFT Calculations. J. Phys. Chem. B 2000, 104 (6), 1300–1306.
- (88) Miller, K. L.; Falconer, J. L.; Medlin, J. W. Effect of Water on the Adsorbed Structure of Formic Acid on TiO₂ Anatase (101). J. Catal. 2011, 278 (2), 321–328.
- (89) Schnadt, J.; Schiessling, J.; O'Shea, J. N.; Gray, S. M.; Patthey, L.; Johansson, M. K. J.; Shi, M.; Krempaský, J.; Åhlund, J.; Karlsson, P. G.; Persson, P.; Mårtensson, N.; Brühwiler, P. A. Structural Study of Adsorption of Isonicotinic Acid and Related Molecules on Rutile TiO₂(1 1 0) I: XAS and STM. Surf. Sci. 2003, 540 (1), 39–54.
- (90) Topalian, Z.; Niklasson, G. A.; Granqvist, C. G.; Österlund, L. Spectroscopic Study of the Photofixation of SO₂ on Anatase TiO₂ Thin Films and Their Oleophobic Properties. ACS Appl. Mater. Interfaces 2012, 4 (2), 672–679.
- (91) Krishnakumar, V.; Mathammal, R. Density Functional and Experimental Studies on the FT-IR and FT-Raman Spectra and Structure of Benzoic Acid and 3,5-Dichloro Salicylic Acid. *J. Raman Spectrosc.* 2009, 40 (3), 264–271.
- (92) Karabacak, M.; Cinar, Z.; Kurt, M.; Sudha, S.; Sundaraganesan, N. FT-IR, FT-Raman, NMR and UV-Vis Spectra, Vibrational Assignments and DFT Calculations of 4-Butyl Benzoic Acid. Spectrochim. Acta - Part A Mol. Biomol. Spectrosc. 2012, 85 (1), 179–189.
- (93) Hoffmann, F. M. Infrared Reflection-Absorption Spectroscopy of Adsorbed Molecules. Surf. Sci. Rep. 1983, 3, 107–192.
- (94) Bao, N.; Gold, J. I.; Szilvási, T.; Yu, H.; Twieg, R. J.; Mavrikakis, M.; Abbott, N. L. Designing Chemically Selective Liquid Crystalline Materials That Respond to Oxidizing Gases. J. Mater. Chem. C 2021, 9 (20), 6507–6517.
- (95) Henkelman, G.; Uberuaga, B. P.; Jónsson, H.; Henkelman, G. A Climbing Image Nudged Elastic Band Method for Finding Saddle Points and Minimum Energy Paths. J. Chem. Phys. 2011, 113 (22), 9900–9904.
- (96) Li, Y.; Gao, Y. Interplay between Water and TiO₂ Anatase (101) Surface with Subsurface Oxygen Vacancy. *Phys. Rev. Lett.* 2014, 112 (20), 1–5.
- (97) Aschauer, U.; He, Y.; Cheng, H.; Li, S. C.; Diebold, U.; Selloni, A. Influence of Subsurface Defects on the Surface Reactivity of TiO₂: Water on Anatase (101). J. Phys. Chem. C 2010, 114 (2), 1278–1284.
- (98) Environmental Protection Agency. Review of the Primary National Ambient Air Quality Standards for Sulfur Oxides;
- (99) Nieuwenhuizen, M. S.; Harteveld, J. L. N. Studies on a Surface Acoustic Wave (SAW) Dosimeter Sensor for Organophosphorous Nerve Agents. Sensors Actuators B Chem. 1997, 40 (2–3), 167–173.

Abstract Graphic

